Longwave radiative forcing of Saharan dust aerosols estimated from MODIS, MISR, and CERES observations on Terra

Jianglong Zhang and Sundar A. Christopher

Department of Atmospheric Sciences, University of Alabama, Huntsville, Alabama, USA

Received 22 August 2003; revised 20 October 2003; accepted 3 November 2003; published 3 December 2003.

[1] Using observations from the Multi-angle Imaging Spectroradiometer (MISR), the Moderate Resolution Imaging Spectroradiometer (MODIS), and the Clouds and the Earth's Radiant Energy System (CERES) instruments onboard the Terra satellite; we present a new technique for studying longwave (LW) radiative forcing of dust aerosols over the Saharan desert for cloud-free conditions. The monthly-mean LW forcing for September 2000 is 7 Wm^{-2} and the LW forcing efficiency (LW_{eff}) is 15 Wm^{-2} per unit aerosol optical depth. Using radiative transfer calculations, we show that simultaneous measurements of the vertical distribution of aerosols, surface temperature and water vapor are critical to the understanding of dust LW aerosol forcing, and must come from other sources. Using well calibrated, spatially and temporally collocated data sets, we have combined the strengths of three sensors from the same satellite to quantify the LW forcing, and show that dust aerosols have a ''warming'' effect over the Saharan desert that will counteract the shortwave ''cooling effect'' of other aerosols. *INDEX TERMS:* 0305 Atmospheric Composition and Structure: Aerosols and particles (0345, 4801); 3359 Meteorology and Atmospheric Dynamics: Radiative processes; 3360 Meteorology and Atmospheric Dynamics: Remote sensing. **Citation:** Zhang, J., and S. A. Christopher, Longwave radiative forcing of Saharan dust aerosols estimated from MODIS, MISR, and CERES observations on Terra, *Geophys. Res. Lett.*, *30*(23), 2188, doi:10.1029/2003GL018479, 2003.

1. Introduction

[2] Desert dust is considered to be one of the major sources of tropospheric aerosol loading, and play an important role in climate forcing studies [*Kaufman et al.*, 2002; *Christopher and Zhang*, 2002]. Widely prevalent in the tropics [*Prospero*, 1999], dust aerosols are effective in reflecting solar energy back to space thereby ''cooling'' the earth's surface [*Tegen et al.*, 1996; *Myhre et al.*, 2003]. Besides their radiative impact in the shortwave portion of the electro-magnetic spectrum, dust aerosols also have an important radiative effect in the longwave (LW) [*Sokolik and Toon*, 1998; *Liao and Seinfeld*, 1998]. Having mean particle sizes on the order of several micrometers [*Dubovik et al.*, 2002], dust aerosols can effectively reduce the earth's LW emission by re-emitting at a colder temperature when compared to the surface and thereby ''warming'' the earth [*Sokolik and Toon*, 1998; *Tegen et al.*, 1996]. However, numerical simulations of dust LW forcing remain a challenging task because of the high spatio-temporal variation of dust properties [*Myhre et al.*, 2003].

[3] Using satellite observations, several studies have attempted to estimate the LW radiative forcing of dust aerosols. For example, using broadband measurements from the Earth Radiation Budget Experiment (ERBE), the changes in LW and shortwave (SW) radiation at the top of atmosphere (TOA) with and without dust aerosols has been reported [e.g., *Ackerman and Chung*, 1992; *Hsu et al.*, 2000]. Since the ERBE instruments were not designed to detect aerosols, narrowband satellite observations from the Advanced Very High Resolution Radiometer (AVHRR) [*Ackerman and Chung*, 1992] and the Total Ozone Mapping Spectrometer (TOMS) [*Hsu et al.*, 2000] were used to identify the presence of dust plumes within the large ERBE scanner footprints. Although the AVHRR and the ERBE scanner were on the same satellite (e.g., NOAA-9), accurate detection of dust aerosols over bright targets such as the Saharan desert was not possible due to the limitations of the AVHRR. The TOMS aerosol index which is the difference in aerosol absorptivity between two UV channels has been used to detect dust aerosols over bright targets such as deserts, but the technique is insensitive to dust layers at low altitudes [*Herman et al.*, 1997] and since the TOMS and ERBE instruments were not on the same satellite, precise temporal collocation was not possible.

[4] With the launch of NASA's Terra satellite, well-calibrated measurements from the same satellite are now available for examining the role of aerosols on climate. For example, using MODIS and CERES data, a first estimate of aerosol radiative forcing over the global oceans has been completed [*Christopher and Zhang*, 2002]. One of the primary roles of the Moderate Resolution Imaging Spectroradiometer (MODIS) and the Multi-Angle Imaging Spectroradiometer (MISR) is to detect aerosols and retrieve their properties. The MODIS with 36 channels has improved spectral, spatial and radiometric resolutions when compared with previous imagers [*King et al.*, 1992] and has been used to retrieve aerosol properties over the global oceans [*Remer et al.*, 2002] and over land areas with low surface reflectances [*Chu et al.*, 2002]. The MISR with multi-angle measurements and four spectral channels has also been used to identify aerosols and retrieve aerosol properties over the global oceans and land including bright targets such as deserts [*Kahn et al.*, 2001]. In this study, we combine the strengths of three instruments on the Terra satellite to examine cloud-free longwave dust aerosol forcing. We use the MODIS to identify clouds because of its multi-spectral capabilities and higher spatial resolution when compared to MISR and CERES. Although the MODIS provides aerosol properties over the global oceans,

0094-8276/03/2003GL018479$05.00

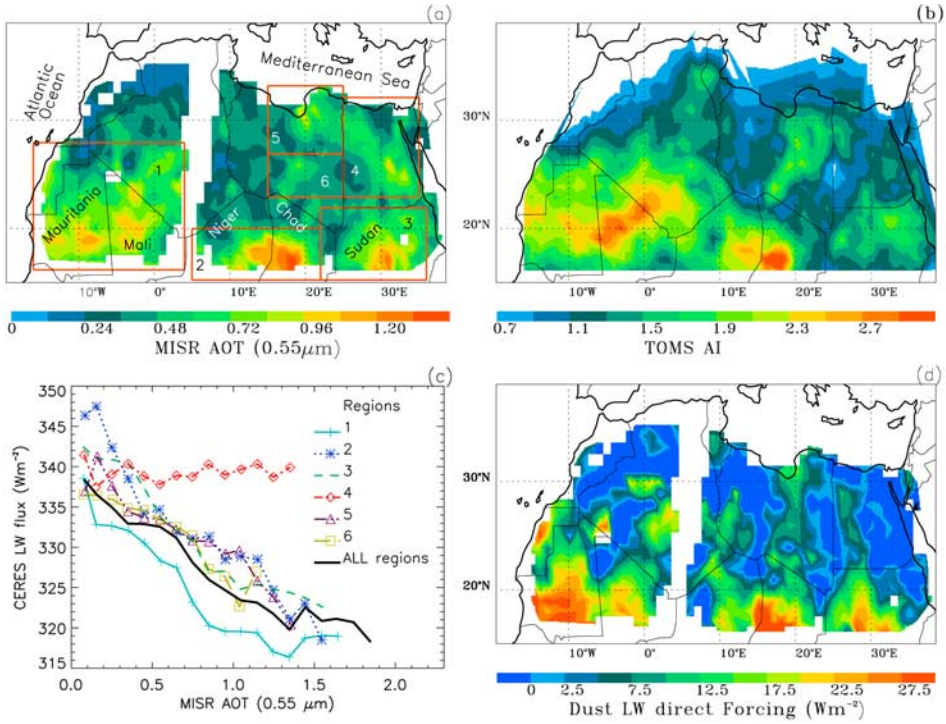

Figure 1. (a) Spatial distribution of MISR optical thickness at 0.55 μm over the area of study for September 2000. Missing data is shown in white and six selected regions (see Table 1) are shown in red boxes, (b) Spatial distribution of the TOMS aerosol index for September 2000, (c) MISR $\tau_{0.55\mu m}$ vs. CERES LW fluxes for the six selected region. Solid black line shows the mean values for the whole region, (d) Spatial distribution of CERES-derived LW direct dust forcing over cloud free desert regions.

aerosol retrievals over highly-reflective surfaces such as deserts are not available. Therefore we use the multi-angle capabilities of the MISR instrument to obtain aerosol optical depth. Finally we use the CERES to obtain broadband TOA longwave fluxes.

2. Data and Methods

[5] Four data sets from September 2000 are used in this study; the MISR Level 2 (MIL2ASAE) 17.6 km daily aerosol product [*Diner et al.*, 2001]; the 5 km MODIS Level 2 daily (MOD06) cloud product [*Ackerman et al.*, 1998] and the 30 km (nadir view) pixel level CERES data [*Wielicki et al.*, 1996]. The MISR aerosol product contains aerosol optical thickness and other related properties at 0.558 μm. The expected uncertainties in MISR aerosol retrievals are ±0.05 for aerosol optical thickness ($\tau_{0.55}$) less than 0.5, and ±10% for $\tau_{0.55}$ greater that 0.5 [*Martonchik et al.*, 1998]. Recently, *Diner et al.* [2001] showed that there was excellent agreement between MISR retrievals and ground based sun-photometer measurements over southern Africa during August and September 2000. The validation of MISR aerosol product over other areas is currently ongoing by the MISR science team. The CERES scanner on Terra observes SW and LW radiances that are converted to fluxes using angular distribution models, which take into account the bi-directional characteristics of a reflecting surface [*Wielicki et al.*, 1996]. Spatial collocation is performed using point spread functions of the CERES scanner [*Christopher and Zhang*, 2002].

[6] The area of study is the Saharan desert (15°–35°N, 18°W–40°E). The CERES pixels that are labeled as "clear desert" by the CERES data were first selected. However, due to the large footprint of the CERES scanner, these pixels could still have some cloud contamination [*Christopher and Zhang*, 2002]. To eliminate these cloud effects, the MOD06 cloud product is collocated with the CERES data and only those CERES pixels that are at least 99.9% cloud free as identified by the MOD06 data were used. Although the MOD06 cloud fraction is aggregated from the 1 km cloud-screening data product using a total of 19 visible and infrared channels [*Ackerman et al.*, 1998], it is possible that thick dust plumes could be misclassified as clouds. For these cloud-free CERES pixels, the best-fit aerosol optical thickness ($\tau_{0.55}$) from the MISR data is obtained. As noted in *Christopher and Zhang* [2002], stringent cloud rejection criteria such as this could eliminate some aerosol plumes that have high optical thickness.

3. Results

3.1. Satellite Observations

[7] Figure 1a shows the monthly-mean MISR $\tau_{0.55}$ for cloud-free CERES pixels. Data is gridded every 1° × 1° and smoothed for display purposes. The major dust plumes are clustered in three regions; within Mali and Mauritania, Chad and Niger, and Sudan. Areas shown in white are due to missing data (Data from September 17, 24, and 30 was not used.), data gaps are also due to cloud-screening criteria. Superimposed on Figure 1a are six selected regions with

Table 1. Summary of MISR Optical Thickness and CERES Fluxes for the Six Selected Regions

Region	Latitude Degrees °N	Longitude Degrees	F_{clr} Wm^{-2}	Dust LW forcing Wm^{-2}	Dust LW direct forcing efficiency[a] Wm^{-2} per $\tau_{0.55}$	$\tau_{0.55}$ (0.55 μm)
1	16–28	16W–4W	338.6	13	20	0.69
2	15–20	5E–22E	346.4	15	21	0.75
3	15–22	22E –36E	342.5	9	19	0.66
4	23–32	25E–35E	341.4	−1	1	0.51
5	27–33	15E–25E	336.8	4	11	0.52
6	23–27	15E–25E	336.5	3	11	0.44
Whole area	15–35	18W–40E		7	15	0.55

[a]Different methods are used in deriving dust LW forcing and LW forcing efficiency (see text). Therefore, the averaged dust LW forcing divided by the averaged $\tau_{0.55}$ may not exactly match the dust LW direct forcing efficiency.

optically thick aerosol plumes. The latitude and longitude boundaries of the six regions are shown in Table 1. For reference purposes, we also compared the spatial distribution of dust aerosols from MISR with those from the TOMS [*Herman et al.*, 1997]. Figure 1b shows the monthly-mean Earth Probe TOMS aerosol index (version 8, level 2) for the same study period. The spatial distribution of dust aerosols derived from these two independent instruments are consistent over most of the study regions. However, over region 4, thick dust plumes shown in Figure 1a are not seen in Figure 1b. Since the TOMS aerosol index is insensitive to dust plumes at low altitudes [*Herman et al.*, 1997], it is possible that these aerosols are not detected by TOMS although we have no ancillary information to verify this. It is also possible that this mismatch is due to the different overpass times of the satellites and the different swath width of these scanners.

[8] Figure 1c shows the MISR aerosol optical thickness versus the CERES LW flux for the six selected regions. For each region, the CERES fluxes are binned for every 0.1 MISR optical thickness intervals, and the bin averaged CERES flux is plotted against MISR $\tau_{0.55}$. The thick black line in Figure 1 shows the mean value for all regions. With the exception of region 4, as MISR $\tau_{0.55}$ increases the CERES LW flux decreases because dust aerosols emit at a colder temperature when compared to the surface. The weak relationship between MISR $\tau_{0.55}$ and CERES LW flux in region 4 is possibly due to the combined effect of dust aerosol vertical distribution, column water vapor, and surface characteristics (see section 3.2). We use this relationship between MISR $\tau_{0.55}$ and CERES LW flux and calculate dust aerosol forcing efficiency for the six selected regions (Table 1). The dust aerosol forcing efficiency (LW_{eff}) is defined as the LW flux perturbation due to dust aerosols per unit optical thickness, and is derived from the difference in CERES LW flux for MISR $\tau_{0.55}$ values between 0 and 1. The largest LW_{eff} of 21 Wm^{-2} per $\tau_{0.55}$ is found over region 2, and the lowest LW_{eff} of 1 Wm^{-2} per $\tau_{0.55}$ is found over region 4. The other four regions have values ranging from 11 to 20 Wm^{-2} per $\tau_{0.55}$. The variability of LW_{eff} is due to differences in surface and atmospheric conditions (see section 3.2). Averaged over all pixels, the regional mean dust aerosol forcing efficiency is 15 Wm^{-2} per $\tau_{0.55}$.

[9] To examine the spatial distribution of the aerosol radiative effect, we define the TOA dust LW forcing as F_{clr} - F_a [*Christopher and Zhang*, 2002], where F_{clr} is the TOA LW flux observed in cloud and aerosol free conditions, and F_a is the TOA LW flux observed over dust regions. For each pixel, the F_{clr} is obtained by averaging the CERES cloud and aerosol free pixels with MISR $\tau_{0.55}$ <0.1 and therefore represents average longwave fluxes for mean atmospheric conditions. Figure 1d shows the dust aerosol LW forcing over the Saharan desert. In general, as $\tau_{0.55}$ increases the LW forcing also increases. However, over region 4, 5, and 6, although dust aerosol loading is high, the aerosol induced LW perturbations are low. The averaged dust aerosol LW direct forcing for the six regions range from −1 to 15 Wm^{-2} (Table 1), and the averaged dust aerosol LW direct forcing over the entire study area is 7 Wm^{-2}. It is interesting to note that over region 4, where MISR observed optically thick aerosols that was not observed by TOMS, the averaged dust LW direct forcing is near zero. It is possible that the dust plume in this region is at a very low altitude and emits at a similar temperature as the surface.

3.2 Sensitivity Studies

[10] Although our analysis clearly shows a longwave "warming" effect, the differences in LW flux as a function of $\tau_{0.55}$ among the six regions are due to both atmospheric and surface properties including surface temperature (T_s), and vertical distribution of water vapor and aerosols [*Hsu et al.*, 2000; *Ackerman and Chung*, 1992]. In this section, we tested the sensitivity of LW_{eff} to changes in T_s, column water vapor, and aerosol vertical distribution over cloud-free desert conditions. A four-stream radiative transfer model [*Fu and Liou*, 1993] was used to compute TOA LW fluxes for various atmospheric and surface conditions with desert aerosol properties as described by *Hess et al.* [1998]. The vertical distribution of dust aerosol extinction is assumed to be exponential, and the dust extinction scale height is used to represent the vertical distribution. For the

Table 2. Dust LW Direct Forcing Efficiency (LW_{eff})[a] as Functions of Surface Temperature, Aerosol Extinction Scale Height and Column Water Vapor From Radiative Transfer Calculations

Surface temperature K	Aerosol extinction scale height km.	Column Water vapor cm.	LW_{eff} Wm^{-2} per $\tau_{0.55}$
316	1	1.6	11.4
316	1	3.2	8.0
316	2	1.6	18.7
316	2	3.2	14.2
300	1	1.6	6.3
300	1	3.2	4.2
300	2	1.6	11.6
300	2	3.2	9.0

[a]Defined as the difference in TOA LW fluxes for $\tau_{0.55}$ values between 0 and 1.

atmospheric temperature and water vapor profiles, we use rawinsonde measurements [27.20°N, 2.47°E] from September 1 at 12 UTC (hereafter referred to as profile 1). The T_s is 316K and the column water vapor is 1.6 cm. To test the sensitivity of T_s, we used another case that has the same water vapor distribution as profile 1, but with different temperature profiles from the surface to 700 mb, The T_s of the new profile (hereafter referred as profile 2) is 300K. We further varied the water vapor amount from 1.6 to 3.2 cm and aerosol extinction scale height from 1 to 2 km.

[11] Table 2 lists the LW_{eff} as functions of aerosol extinction scale height, T_s and column water vapor. The profiles 1 and 2 are identified by their surface temperatures of 316K and 300K respectively. When the dust aerosol scale height is changed from 1 to 2 km while keeping the surface temperature (316K) and the water vapor loading the same (1.6 cm), the LW_{eff} increases from 11.4 to 18.7 Wm^{-2} per $\tau_{0.55}$, because the dust layer now emits at a colder temperature and consequently, water vapor absorption above the dust layer is reduced. Increasing the water vapor loading from 1.6 to 3.2 cm for the same temperature (316K) and aerosol extinction height (1 km) reduces the LW_{eff} from 11.4 to 8.0 Wm^{-2} per $\tau_{0.55}$ because the absorption due to water vapor above the dust layer has increased. Increasing the surface temperature from 300 to 316 K for the same water vapor loading (1.6 cm) and aerosol scale height (1 km) will increase the LW_{eff} from 6.3 to 11.4 Wm^{-2} per $\tau_{0.55}$ because the cloud and aerosol free emission temperature increases. Averaged over all eight cases, while holding other surface and atmospheric parameters constant, a 10% variation in column water vapor loading (at 1.6 cm) could produce 2–3% uncertainties in LW_{eff}. Note that in our LW_{eff} calculations, we assume that the column water vapor values are the same for clear and dusty conditions. However, a 10% variation in column water vapor between clear and dusty skies could produce much large uncertainties in LW_{eff}. In summary, LW_{eff} is proportional to T_s and aerosol extinction scale height, and inversely proportional to water vapor content. All three of these parameters are critical to the understanding of LW dust direct forcing, and precisely collocated observations of the three parameters from other sources are needed for future dust forcing studies that utilize broadband satellite observations.

4. Summary

[12] In this paper, we have demonstrated a new technique for estimating the dust aerosol LW direct forcing over the Saharan desert. Through the synergistic use of MODIS, MISR and CERES instruments onboard the same satellite, our study clearly shows that there is a strong dust warming effect of 7 Wm^{-2} over the cloud free Sahara desert regions for September 2000 that can offset the shortwave cooling effect of other aerosols. The regional mean dust LW direct forcing efficiency is 15 Wm^{-2} per $\tau_{0.55}$. However, since water vapor dominates the radiative processes in the longwave part of the electromagnetic spectrum, simultaneous measurements of both aerosol height and column water vapor are needed to reduce the uncertainties in the longwave radiative forcing calculations of dust aerosols.

[13] **Acknowledgments.** This research is supported by NASA's Radiation Sciences, Interdisciplinary Sciences and ACMAP programs. Jianglong Zhang is supported by the NASA Earth System Science Fellowship. The CERES and MISR data were obtained from the NASA Langley Research Center Atmospheric Sciences Data Center and the MODIS data were obtained through the Goddard Space Flight Center Data Center. We also thank the CERES science team for providing the CERES point spread function and geolocation information. We thank Dr. Clark Weaver for his suggestions during the preliminary stages of this research.

References

Ackerman, S. A., and H. Chung, Radiative effects of airborne dust on regional energy budgets at the top of the atmosphere, *J. Appl. Meteorol.*, *31*, 223–233, 1992.

Ackerman, S. K., Strabala, P. Menzel, R. Frey, C. Moeller, and L. Gumley, Discriminating clear sky from clouds with MODIS, *J. Geophys. Res.*, *103*, 32,141–32,157, 1998.

Christopher, S. A., and J. Zhang, Shortwave Aerosol Radiative Forcing from MODIS and CERES observations over the oceans, *Geophys. Res. Lett.*, *29*(18), 1859, doi:10.1029/2002GL014803, 2002.

Chu, D. A., Y. J. Kaufman, C. Ichoku, L. A. Remer, D. Tanré, and B. N. Holben, Validation of MODIS aerosol optical depth retrieval over land, *Geophys. Res. Lett.*, *29*(12), 8007, doi:10.1029/2001GL013205, 2002.

Diner, D. J., W. A. Abdou, J. E. Conel, K. A. Crean, B. J. Gaitley, M. Helmlinger, R. A. Kahn, J. V. Martonchik, and S. H. Pilorz, MISR aerosol retrievals over southern Africa during the SAFARI-2000 dry season campaign, *Geophys. Res. Lett.*, *28*, 3127–3130, 2001.

Dubovik, O., et al., Variability of absorption and optical properties of key aerosol types observed in worldwide locations, *J. Atmos. Sci.*, *59*, 590–608, 2002.

Fu, Q., and K. N. Liou, Parameterization of the radiative properties of cirrus clouds, *J. Atmos. Sci.*, *50*, 2008–2025, 1993.

Herman, J. R., P. K. Bhartia, O. Torres, C. Hsu, C. Seftor, and E. Celarier, Global distribution of UV-absorbing aerosols from Nimbus 7/TOMS data, *J. Geophys. Res.*, *102*, 16,911–16,922, 1997.

Hess, M., P. Koepke, and I. Schult, Optical properties of aerosols and clouds: The software package OPAC, *B. Am. Meteorol. Soc.*, *79*, 831–844, 1998.

Hsu, N. C., J. R. Herman, and C. Weaver, Determination of radiative forcing of Saharan dust using combined TOMS and ERBE data, *J. Geophys. Res.*, *105*, 20,649–20,661, 2000.

Kahn, R., P. Banerjee, and D. McDonald, The sensitivity of multi-angle imaging to natural mixtures of aerosols over ocean, *J. Geophys. Res.*, *106*, 18,219–18,238, 2001.

Kaufman, Y. J., D. Tanre, and O. Boucher, A satellite view of aerosols in the climate system, *Nature*, *419*, 215–223, 2002.

King, M. D., Y. J. Kaufman, W. P. Menzel, and D. Tanre, Remote Sensing of Cloud, Aerosol, and Water Vapor Properties from the Moderate Resolution Imaging Spectrometer (MODIS), *IEEE Trans. Geosci. Rem. Sens.*, *30*, 2–27, 1992.

Liao, H., and J. H. Seinfeld, Radiative forcing by mineral dust aerosols: Sensitivity to key variables, *J. Geophys. Res.*, *103*, 31,637–31,645, 1998.

Martonchik, J. V., D. J. Diner, R. A. Kahn, T. P. Ackerman, M. M. Verstraete, B. Pinty, and H. R. Gordon, Techniques for the retrieval of aerosol properties over land and ocean using multiangle imaging, *IEEE Trans. Geosci. Rem. Sens.*, *36*, 1212–1227, 1998.

Myhre, G., et al., Modeling the radiative impact of mineral dust during the Saharan Dust Experiment (SHADE) campaign, *J. Geophys. Res.*, *108*(D18), 8579, doi:10.1029/2002JD002566, 2003.

Prospero, J. M., Long-term measurements of the transport of African minerals dust to the southeastern United States: Implications for regional air quality, *J. Geophys. Res.*, *104*, 15,917–15,928, 1999.

Remer, L. A., D. Tanré, Y. J. Kaufman, C. Ichoku, S. Mattoo, R. Levy, D. A. Chu, B. Holben, O. Dubovik, A. Smirnov, J. V. Martins, R. R. Li, and Z. Ahmad, Validation of MODIS aerosol retrieval over ocean, *Geophys. Res. Lett.*, *29*(12), 8008, doi:10.1029/2001GL013204, 2002.

Sokolik, I. N., and O. B. Toon, Modeling the radiative characteristics of airborne mineral aerosols at infrared wavelengths, *J. Geophys. Res.*, *103*, 8813–8826, 1998.

Tegen, I., A. A. Lacis, and I. Fung, The influence on climate forcing of mineral aerosols from disturbed soils, *Nature*, *380*, 419–422, 1996.

Wielicki, B. A., B. R. Barkstrom, E. F. Harrison, R. B. Lee III, G. L. Smith, and J. E. Cooper, Clouds and the Earth's Radiant Energy System (CERES): An Earth Observing System Experiment, *B. Am. Meteorol. Soc.*, *77*, 853–868, 1996.

S. A. Christopher and J. Zhang, Department of Atmospheric Sciences, NSSTC, University of Alabama in Huntsville, 320 Sparkman Drive, Huntsville, AL 35806, USA. (sundar@nsstc.uah.edu)